Low-THz Overhead Power Cable Signatures

Willetts, Ben; Gashinova, Marina; Stove, Andrew; Constantinou, Constantinos; Hoare, Edward; Marchetti, Emidio

Low-THz Overhead Power Cable Signatures

The effect of surface features on Low-THz reflectivities

B. Willetts, M. Gashinova, A. Stove, C.C. Constantinou, E.G. Hoare, E. Marchetti
Microwave Integrated Systems Laboratory
University of Birmingham
Birmingham, UK
bxw942@bham.ac.uk, m.s.gashinova@bham.ac.uk, stovea@adf.bham.ac.uk,
c.constantinou@bham.ac.uk, e.g.hoare@bham.ac.uk, exm486@bham.ac.uk

Abstract—**The measurements presented in this paper show that feature extraction can be used to identify objects of interest by making use of the scattering present and angular resolution available when using low TeraHertz (low-THz) (0.1 THz-1 THz) devices. The results shown were obtained by measuring two different types of overhead power cables of similar size but with different surface structure which causes the backscatter from each type of cable at 150GHz to be distinct. The measurements are supported by simulations made that incorporate Bragg mode theory.**

Index Terms— **Low-THz, Rough surface, Radar imaging, Radar cross-section, Electromagnetic reflection**

I. Introduction

Interest in the millimetre wave (MMW) and TeraHertz (THz) band of frequencies is increasing due to the inherent advantages of such systems over devices that operate at longer wavelengths, including increased angular resolution for a given antenna size, more compact devices and higher range resolution [1].

A target that is of particular interest is the overhead (OH) power cable. These power cables were previously measured by using radar devices that make use of larger wavelengths but the backscatter amplitudes measured were deemed inadequate to allow a high enough probability of detection in practical situations [2].

The most common type of overhead conductor is the Aluminium Conductor Steel Reinforced type.(ACSR) which typically consists of exposed aluminium strands of cylindrical wire, helically wrapped around a steel core (top in Fig 1). The number of strands of wire present depends on the current capacity of the cable. The Aluminium Conductor Composite Core (ACCC) type (bottom in Fig 1) of power cable is the modern, more efficient type of overhead cable that is becoming increasingly popular as it can carry higher currents for a given weight compared to the older ASCR type; meaning the ACCC type incurs less mechanical sag after installation. To the best of our knowledge the scattering measurements presented here are the first ever reported for the ACCC type of cable.

The grating lobes of the ACSR cable surface are considered to be the most important feature in terms of its backscatter for low-THz remote sensing as the dimension of these features is comparable to a wavelength at low-THz frequencies.

Several sets of measurements of ACSR cables at multiple microwave frequencies have been reported previously [3] [4]. Previous research show that below typically 30 GHz the scattering of this type of cable is very similar to that of a smooth metallic cylinder as the cable surface details do not significantly alter the scattering present at these wavelengths. The previous behaviour means the amplitude of the backscattered energy is only large for a narrow range of incident angles. The scattering behaviour at low frequencies makes the power cable hard to detect especially by a moving aircraft equipped with a monostatic radar device.

In the frequency range 35 GHz to 94 GHz the physical helical features of typical OH power cables are comparable to the wavelength leading to the presence of additional reflection Bragg lobes with peaks at certain incident angles (θ_n) caused by Bragg mode scattering:

$$|\theta_n| = \sin^{-1}\left(\frac{n\lambda}{2L}\right) \qquad n=1,2,3.... \qquad (1)$$

The position of these extra peaks thus depends on the ratio of the wavelength (λ) of the incident electromagnetic wave to the surface period (L) of the cable [2] (Fig 2). This feature depends on the type of ACSR cable. This behaviour broadens the range of angles at which strong backscatter occurs compared to operation at lower frequencies and helps the detection and identification of power cables. The previous Bragg scattering is still specular in nature at 35 GHz and 94 GHz and previous research has shown that the scattered energy resides almost entirely in the Bragg lobes. These lobes extend out to an angle α either side of broadside as shown in [3], α depends on the cable size (D) and spacing between turns (P):

$$|\alpha| < \tan^{-1}\left(\frac{\pi D}{P}\right) \qquad (2)$$

For typical cable geometries; α is around 15°.

Measurements of OH power cable have also been reported at two different IR wavelengths (1.06 μm and 10.6 μm) [3] [5]. The Bragg mode peaks seen at lower frequencies were not distinguishable in all IR measurements but the majority of the backscatter is still found relatively close to normal incidence for the undamaged cables that were measured.

The motivation for performing measurements on ACSR cables at 150 GHz is to find out whether the pattern of Bragg modes persists at shorter wavelengths, but with a denser set of returns, and/or whether the shorter wavelength means that diffuse scattering becomes more significant. The further motivation for measuring the ACCC cables was to see whether the smoother surface still had sufficient structure to allow features to be extracted.

The beam widths available at low-THz frequencies are expected to provide sufficient angular resolution at short ranges to allow the expected Bragg modes to be separable by imaging a cable along its length and this too is of interest in the research.

A parameter which becomes more important as the range increases is the scattering loss which is due to the presence of smoke or dust particles which can exist in rescue/hostile environments. This scattering loss caused by the presence of airborne particles is lower for THz devices compared to the loss present for Infrared (IR) and optical wavelengths [6] .The previous is expected to make low-THz devices more suitable for the detection of targets, such as overhead power cables, in outdoor environments even though these higher bands of frequencies have inherent advantages such as narrower beam widths and devices with smaller dimensions.

The next section states the parameters of the radar device used in experiments and also the geometric characteristics of the cables measured. Section III puts across the experimental scenario realised, Section IV displays simulated results and the results obtained experimentally are then presented and discussed in Section IV.

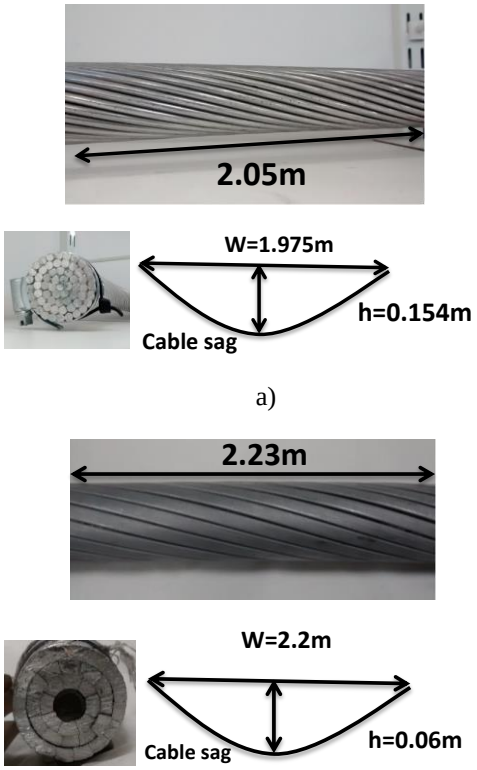

Figure 1. a) ACSR and b) ACCC surface pattern and cable sag

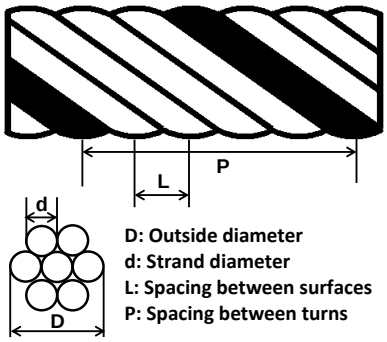

Figure 2. Physical parameters of a helically wound cable

II. Experimental Setup

The characteristics of the ACSR and ACCC types of overhead power cable measured are shown in Table 1. The expected values of θ_1 and α for the ACSR cable were 2.9 ° and ±15°, respectively and for the ACCC, 2.3° and 15°, respectively.

All the measurements presented here were obtained by using a 150 GHz FMCW monostatic radar system [7]. The imaging experiments were performed by using lens horn antennas at the Receive and Transmit terminals. Table 2 shows the important parameters for the radar device and antennas used.

TABLE I. Cable parameters for both types of cables measured

Cable Parameter (ACSR)	**Value**	**Cable Parameter (ACCC)**	**Value**
Cable diameter (*D*)	31.59 mm	Cable diameter(*D*)	33.4 mm
Number of outer strands	24	Number of outer strands	16
Outer surface period (*L*)	20 mm	Outer surface period (*L*)	24.37 mm
Length between turns (*P*)	355.6 mm	Length between turns (*P*)	390 mm
Cable length	2.05 m	Cable length	2.23 m
Outer strand diameter (*d*)	3.51 mm	Trapezoidal Outer Strand	

TABLE II. Parameters of 150GHz radar device & antennas used

Parameter	**Quantity**
Frequency Band	144-150 GHz
Range Resolution	30 mm
Transmit Power	11dBm
Antenna Gain (RX/TX)	29dBi
3dB beamwidth (E-plane)	15°
3dB beamwidth (H-plane)	2.2°

III. Power Cable Imaging Setup

The imaging of both the ASCR and ACCC cables were performed in an indoor environment (Fig 3). The range of the background clutter in the scanning area was measured and range gating was possible to eliminate it. The illumination (3 dB beam width) of the cable with the lens horn antennas had a span of approximately 50 mm (H-plane) by 342 mm (E-plane) as each target was located approximately 1.3m in range from the antenna configuration. The cable was imaged by mechanically scanning the radar system in the H-plane/azimuth plane with an increment angle of 1.1° and the total scanned angle was ±20° for two different scenarios (Fig 4 and Fig 5). Each measurement shown is the result of averaging over 5 measurement samples.

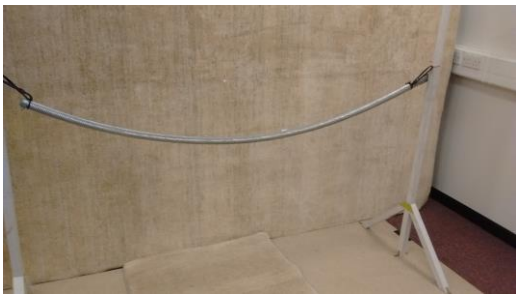

a)

b)

Figure 3. Setup for overhead power cable imaging experiments - a) ACSR b)ACCC

IV. Overhead Power Cable Simulations

Bragg mode theory was used to simulate the behaviour that would be present when scanning a periodically structured power cable.

Isotropic radiators with a RCS magnitude of unity were placed at the locations predicted by Bragg theory (Eq 1) with the monostatic radar located in the same location as in experiments; assuming perfect alignment. The antenna pattern was simulated using a Gaussian beam shape (Eq 3) [8] and the cable sag was introduced by using the equation for a parabola (Eq 4) [9] and the cable parameters shown in Fig 1 for both cables. The produced scenario is shown in Fig 6 for the ASCR cable.

The received power was then calculated using the radar equation (Eq 5). The realised maximum power plots are shown in Fig 7-10 for both types of cables and for both imaging scenarios.

The simulated results show periodic peaks with the ACSR cable being more pronounced with the peaks and troughs having a larger variation compared to the ACCC type. The cut-off angle for strong backscatter is around 16° for all simulations. The largest Bragg lobe peak for both cables is located at 0° in the case of scenario 1 and then shifts to the negative cut-off angle for scenario 2.

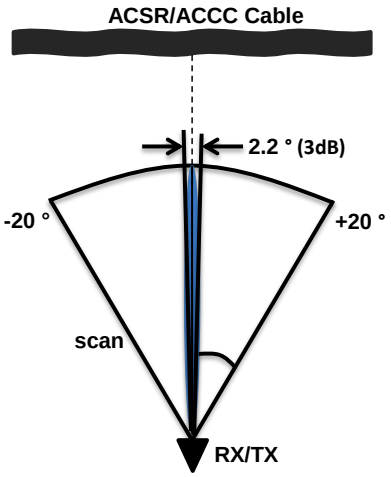

Figure 4. Scenario 1 in overhead power cable imaging experiments

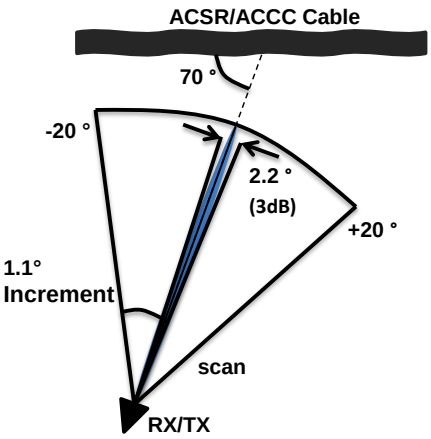

Figure 5. Scenario 2 in overhead power cable imaging experiments

$$G_n(\theta) = \exp\left[-0.694\left(\frac{\theta}{\theta_0}\right)^2\right] \tag{3}$$

$$y(x) = h\left(\frac{2x}{W}\right)^2 \tag{4}$$

$$P_r[dBW] = P_t[dBW] + 2G_{tx/rx}[dBi] + \sigma[dBsm] + 20\log(\lambda) - 30\log(4\pi) - 40\log(R[Range]) \quad (5)$$

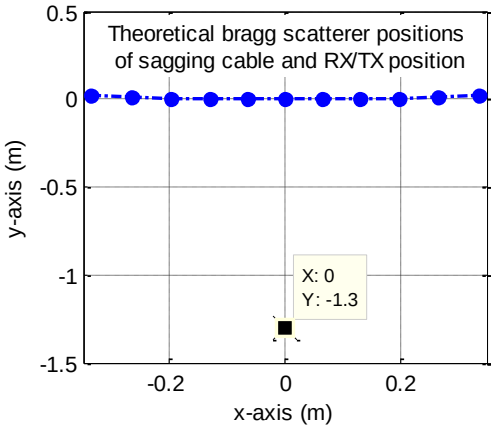

Figure 6. Simulation scenario with isotropic radiators at the expected Bragg mode angles and the location of the monostic radar transeiver

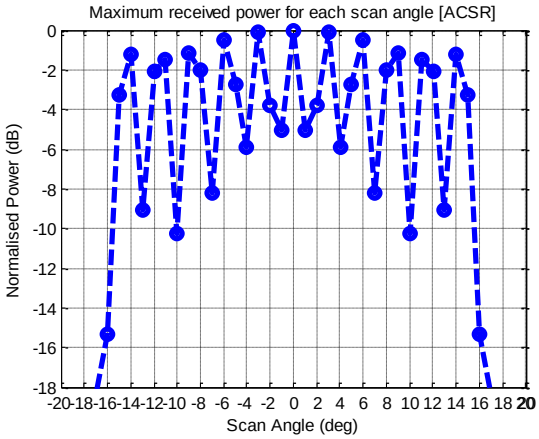

Figure 7. The maximum power in simulations for each scan angle [ASCR] (Scenario 1)

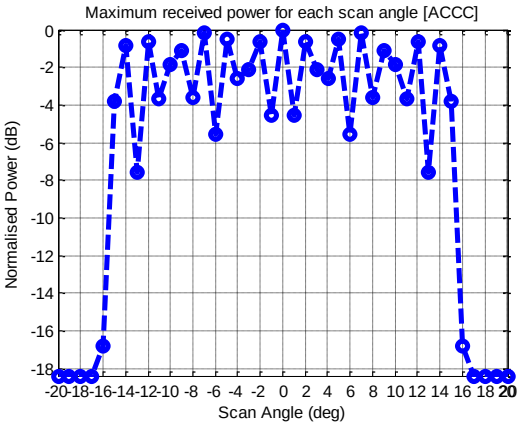

Figure 8. The maximum power in simulations for each scan angle [ACCC] (Scenario 1)

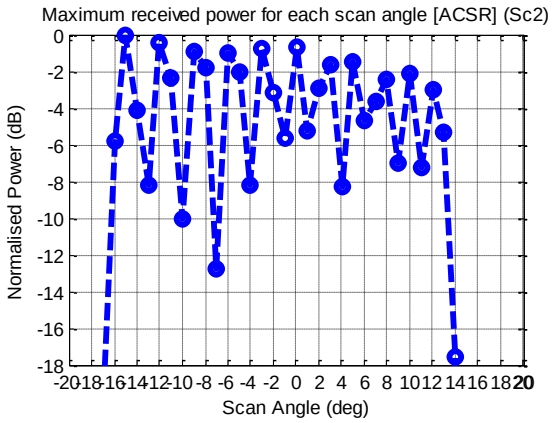

Figure 9. The maximum power in simulations for each scan angle [ACCC] (Scenario 2)

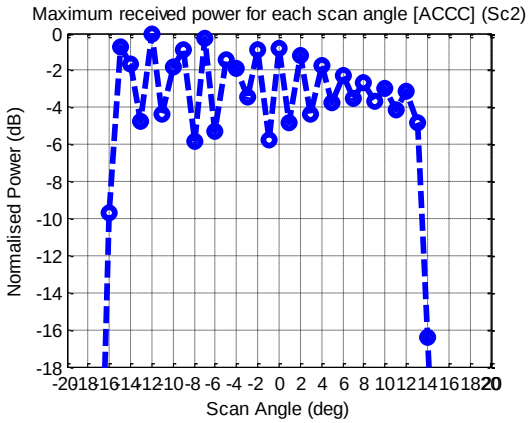

Figure 10. The maximum power in simulations for each scan angle [ACCC] (Scenario 2)

V. Overhead Power Cable Measurements

The images obtained from scanning the ACSR type of cable are visible in Fig 11 and Fig 12 whilst the images obtained by imaging the ACCC type are visible in Fig 13 and Fig 14. The plots of the maximum power return for each angle measured for each cable type and scenario are shown in Fig 15-18.

The Bragg mode behaviour was qualitatively as expected for the ACSR cable, with periodic peaks being present at certain angles although some peaks seem to be missing. Theory predicted 11 Bragg lobe peaks with an angular separation of 2.9°, as in Fig 7 and Fig 8, although in Fig 10 only 6 peaks are present which are separated by an angle in the range of 4.4° to 6.6°. The absence of Bragg lobes is currently under investigation although the illumination properties, effect of range resolution and cable imperfections in the realised experiment are all expected to cause a deviation

from theory. The shift in the largest Bragg mode peak observed in simulations was also seen in measurements for the two different scenarios.

The flatter trapezoidal strands present for the ACCC type seem to have suppressed most of the higher order Bragg mode peaks and the measured results deviate significantly from Fig 8.

Measurements at lower frequencies [4] showed essentially no diffuse scattering, but these measurements show a 'background' RCS level which is what would be expected from diffuse scattering.

Until further investigations are conducted we postpone making definitive statements about the apparent deviation from Bragg theory or about the possible diffuse scattering present because both effects may also be associated with the very short range at which these measurements were made.

The presence of scattering over relatively wide angles shows that the use of low-THz frequencies, used to build compact systems, would still allow cable detection and classification by scanning mechanically with a narrow-beam antenna without the need for excessively complex post processing.

VI. Conclusion

Results have been presented of the backscatter from overhead power cables at frequencies that have not been measured before. As well as measurements on the traditional standard (ACSR) cables, results have also been shown of the newer ACCC type of cables.

The results for the ACSR are broadly in agreement with what would be predicted from the models which have proved successful at lower, millimetre-wave and centimetre-wave frequencies, but there is some evidence of more complex behaviour. Some of the expected Bragg peaks seem to be missing and this merits further investigation.

For the ACCC cables the same models are probably still the best starting point for predicting the performance, but the deviations are now very significant – many expected modes seem to be of low amplitude or missing. Some are also much wider than would have expected, which is compatible with the effective length of the illuminated section of the wire being lower than expected.

Acknowledgment

We would like to thank the National Grid Power Systems Research Centre at the University of Manchester for the donation of the overhead power cables used in the research.

References

[1] A. Stove, "Potential applications for low-Tera-Hertz radar," in Radar Symposium (IRS), 2015 16th International , vol., no., pp.191-196, 24-26 June 2015.

[2] K. Sarabandi; M. Park, "Millimeter-Wave Radar Phenomenology of Power Lines and a Polarimetric Detection Algorithm," IEEE Transactions on Antennas and Propagation, Vol. 47, No. 12, 1999.

[3] H. Al- Khatib, "Laser and millimeter-wave backscatter of transmission cables," Proc. SPIE 0300, Physics and Technology of Coherent Infrared Radar I, 212 ,1981.

[4] W.M. Polivka, "Power line: radar measurement and detection algorithm for polarimetric SAR images," IEEE Transactions on Aerospace and Electronic Systems, Vol. 30, No.2, 1994.

[5] C. L. Hayes; R.A. Brandewie, "Reflection Coefficients for Wires and Cables at 10.6μm," Applied Optics, Vol. 12, No. 7, 1973.

[6] M.J. Fitch; R. Osiander, "Terahertz Waves for Communications and Sensing," Johns Hopkins APL Technical Digest, Vol 25, No 4, 2004.

[7] D.R. Vizard; M. Gashinova; E.G. Hoare; D Jasteh.; L Daniel; M Cherniakov; T-Y Tran ; N Clarke, "Antenna range evaluations of low THz imagers for automotive applications," Antenna Measurements & Applications (CAMA), 2014 IEEE Conference on , pp.1-4, 2014.

[8] D.P. Meyer; H.A. Mayer, "Radar Target Detection: Handbook of Theory and Practice", pp. 77, Academic Press, 1973.

[9] W.J. Lewis, "A Mathematical Model for Assessment of Material Requirements for Cable Supported Bridges: Implications for Conceptual Design.". 2012.

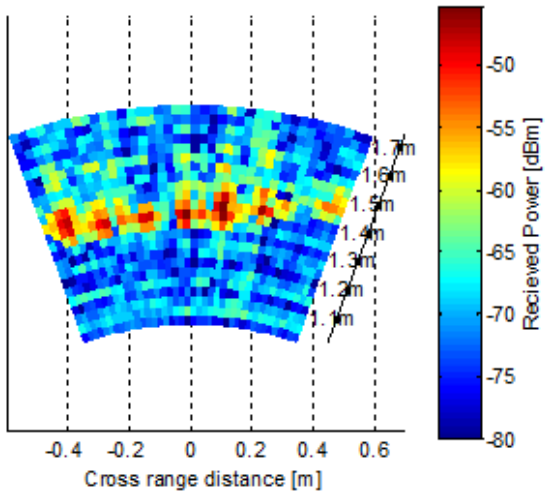

Figure 11. Image obtained by imaging ACSR cable [scenario 1]

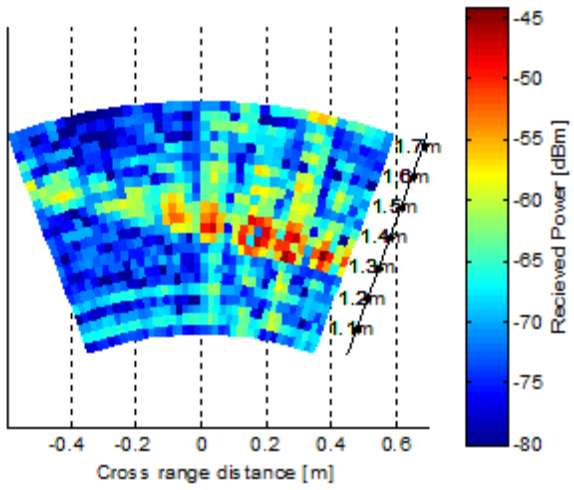

Figure 12. Image obtained by imaging ACSR cable [scenario 2]

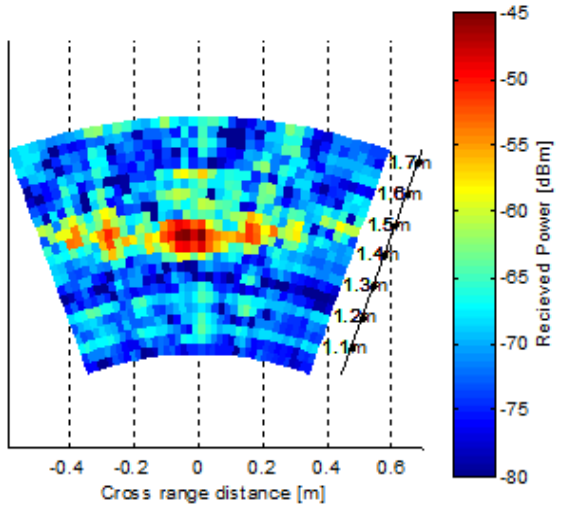

Figure 13. Image obtained by imaging ACCC cable [scenario 1]

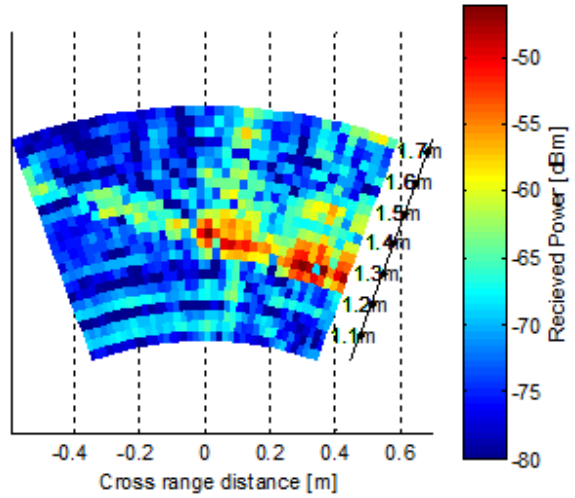

Figure 14. Image obtained by imaging ACCC cable [scenario 2]

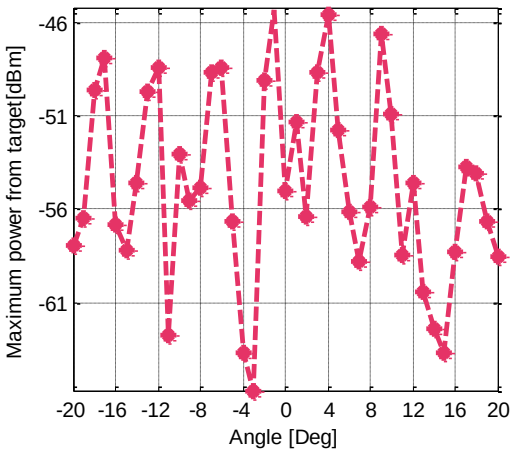

Figure 15. Maximum power at each angle by imaging ACSR cable [scenario 1]

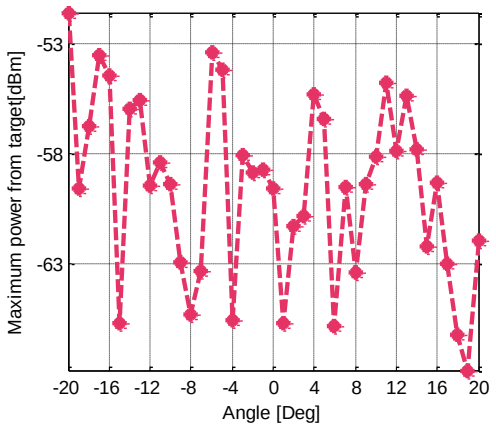

Figure 16. Maximum power at each angle by imaging ACSR cable [scenario 2]

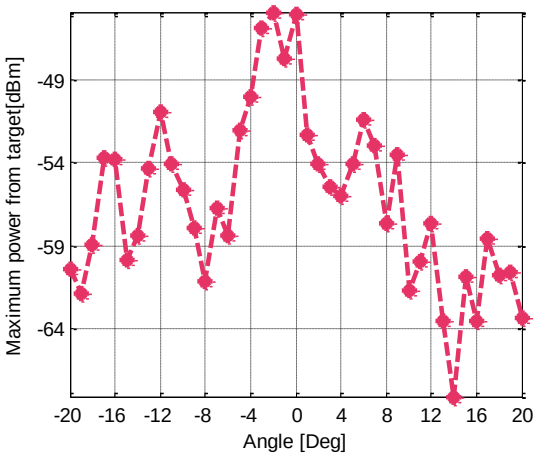

Figure 17. Maximum power return at each angle by imaging ACCC cable [scenario 1]

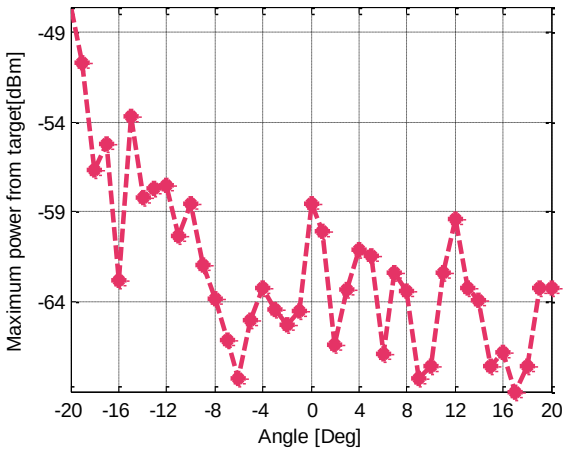

Figure 18. Maximum power return at each angle by imaging ACCC cable [scenario 2]